Inorganic Chemistry Communications 155 (2023) 111073

Contents lists available at ScienceDirect

Inorganic Chemistry Communications

journal homepage: www.elsevier.com/locate/inoche

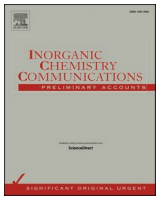

Short communication

Effect of fluoric acid concentration on the structural, optical, and photocatalytic properties of TiO_2 thin films

Abdelaziz Abboudi [a], Sabrina Iaiche [b], Abdelkader Djelloul [b], Abdelouahed Chala [c], Fouzi Kezzoula [d], Fayçal Bensouici [b], Mohamed Bououdina [e,*], Muhammad Humayun [e,*]

[a] Laboratory of Engineering and Advanced Materials Science (ISMA), Faculty of Sciences and Technology, Abbes Laghrour University, Khenchela 40.000, Algeria
[b] Laboratory of Structures, Properties and Interatomic Interactions LASPI2A, Department of Matter Sciences, Faculty of Sciences and Technology, Abbes Laghrour University, Khenchela 40.000, Algeria
[c] Laboratoire de physique des couches minces et applications, BP 145 RP, Université de Biskra
[d] CRTSE, 02, Bd. Dr Frantz FANON, B.P. 140 Alger-7, Merveilles 16038, Algeria
[e] Energy, Water, and Environment Lab, College of Humanities and Sciences, Prince Sultan University, Riyadh 11586, Saudi Arabia

ARTICLE INFO

Keywords:
Fluorine
Titanium oxide
Organic dye
Thin films
Photocatalysis

ABSTRACT

In this work, we have successfully fabricated bare titanium oxide (TiO_2) and fluorine (F) doped TiO_2 thin films via the sol–gel dip-coating technique on the soda lime glass substrates. The effect of hydrofluoric acid (HF) concentration on the structural, optical, and photocatalytic properties of TiO_2 thin films is investigated. The films are characterized by the X-ray diffraction (XRD) technique, scanning electron microscopy (SEM), X-ray photoelectron spectroscopy (XPS), energy dispersive X-ray spectroscopy (EDS), atomic force microscopy, and UV–visible spectrophotometer. The XRD patterns show the presence of highly crystalline anatase phase TiO_2. The SEM images reveal some cracked surfaces, while the EDX reveals the absence of fluorine in all samples. The AFM images exhibit a decrease in roughness with the increase in HF concentration. UV–visible spectrometry reveals high transparency in the visible region (about 85%) and the shift in absorption edge toward the higher energy side. To evaluate the photocatalytic performance of the photocatalysts, methylene blue (MB) dye is chosen as a model pollutant. The photocatalytic test shows a decrease in the degradation rate of MB with the increase in HF concentration in the solution. This work will trigger the development of highly efficient acid-modified photocatalysts for environmental remediation.

1. Introduction

Environmental cleanup is one of today's most hotly debated issues. Economic activity in both industrialized and developing nations has a significant impact on the quality of air and water [1–6]. Titanium dioxide (TiO_2) is a stable and cheap material widely used as a promising material for organic pollutant degradation due to its unique properties [7–9]. Many attempts have been made over the last few years to solve the two key issues involving the low performance of the photo-oxidative process, which competes with photo-induced electron-hole pair recombination, and the considerably large band gap energy (3.2 eV), which usually requires the utilization of UV light energy for excitation of electrons from the valence band to the conduction band of semiconductors. In this case, the researcher provided numerous approaches to boost the photocatalytic performance of TiO_2 [8,10].

Doping among numerous strategies is one of the key techniques employed to modify the Fermi level. The doping technique in photocatalysts consists of a direct tuning of the band gap structure by producing additional energy levels in order to enhance light absorption and also build carrier trap sites to avoid fast recombination [11]. Many researchers doped transition metal elements like Cu [12], Ag [13], Fe [14], Al [15], and Au [16,17] in TiO_2. Some researchers doped non-metal elements like C [18,19], N [20,21], P [22,23], S [24,25], B [26,27], and F [28,29] into TiO_2 and the resultant photocatalysts have shown significant improvement in the light absorption toward visible light region.

Regarding doping with non-metallic elements, three proposed excitation mechanisms are discussed. For instance, Morikawa et al. [30] proposed a band gap narrowing mechanism, Irie et al. [31] proposed an impurity energy level mechanism, and Ihara et al. [32] presented an

* Corresponding authors.
E-mail addresses: mbououdina@psu.edu.sa (M. Bououdina), mhumayun@psu.edu.sa (M. Humayun).

https://doi.org/10.1016/j.inoche.2023.111073
Received 16 April 2023; Received in revised form 4 July 2023; Accepted 11 July 2023
Available online 13 July 2023

oxygen vacancy mechanism. Modification of TiO_2 with fluorine is of great significance and attracted worldwide scientific attention. For example, Minero et al. [33] demonstrated that the photocatalytic performance of TiO_2 for degradation of phenol in presence of fluoride ions was enhanced by 3-fold compared to that of the bare TiO_2. Thus, fluorine doping, followed by calcination at high temperature, increases the surface trap sites, which are beneficial for the enhanced photocatalytic activity [7]. Some researchers demonstrated that F also reduces the hole diffusion from the bulk to the surface of TiO_2 and also inhibit charge recombination. As a result, the F:TiO_2 performs as an exceptional photocatalyst [34,35]. This enhancement in the photocatalytic activity can be explained by the fact that the fluoride dopant enhances surface acidity of the catalyst and create the reduced Ti^{3+} ions because of the charge compensation between Ti^{4+} and F^- ions. In particular, fluorination has been found to reduce the hydrophilicity of TiO_2 and shift the site of zero charges of TiO_2 towards lower pH levels [36]. Also, it is found that fluorine increases the anatase phase stability, facilitates the formation of surface defects [7], and narrows the band gap of TiO_2 [37]. Thus, it is of great significance to modify TiO_2 with fluoride ions.

Herein, we have successfully fabricated pure TiO_2 and fluorine doped TiO_2 thin films via a sol–gel and dip-coating techniques. Various characterization of the photocatalysts are carried out in order to investigate the affect of fluoride ions on the structural, surface morphological, optical, and photocatalytic properties of TiO_2. The photocatalytic test reveals a decrease in the degradation rate of MB with the increase in hydrofluoric acid (HF) concentration. This work will trigger the development of various dopants modified photocatalysts for environmental remediation.

2. Experimental section

2.1. Films fabrication

For the fabrication of un-doped and F-doped TiO_2 films, a facile and low-cost sol–gel dip-coating method was adopted. The precursor tetraethyl-orthotitanate (Merck 95% purity) was dissolved in a mixture of ethanol, nitric acid (Sigma-Aldrich 69% purity) and water. The solution was swirled repeatedly for 1 h. After aging the solution for roughly 24 h, the films were deposited onto the glass substrates via a dip-coater with a withdrawing speed of 1 mm/s. The dipping number indirectly regulated the thickness of the deposited layer [14]. The F-doped TiO_2 sol was made using the same method as described above. The only difference was that hydrofluoric acid (HF) (sigma Aldrich 48%) was added to the TiO_2 sol as a source of fluoride ions. The F concentration was varied as follows: 0, 7, 14, and 21% molar ratio, respectively.

2.2. Films characterization

The crystallinity of TiO_2 films was measured using the X-ray diffraction (XRD) technique in thin film mode on a X'PERT MPD Philips diffractometer with CuKα radiation source (λ = 1.5406). The XPS analysis was performed by the "Thermo Scientific ESCALAB Xi" spectrometer from thermo-fisher using Al-Kα X-ray beam of 7.6 kW (photon energy = 1486.8 eV) in pressure of 5 x10^{-10} mBar and operating energy of 200 eV. Optical transmittance was determined at normal incidence in the UV–Vis-NIR spectra region of 190–1100 nm, using a Spectro Scan 80D spectrophotometer. Surface topography was examined using an atomic force microscope from MFP3D Asylum Research and Oxford Instrument (AFM). The SEM pictures were obtained using a high-performance analytical SEM Tescan VEGA3 equipped with a high-count rate silicon drift EDS system, capable of working in both high and low vacuum modes.

2.3. Photocatalytic measurements

A homemade device was used to evaluate photocatalytic performance. It was measured by oxidizing a water diluted MB dye solution. About, 35 mL of the MB solution with initial dye concentration of 2.5 10^{-5} mol/L was placed in a UV-transparent glass cell (capsule with a round bottom having a diameter of 45 mm). The as-fabricated samples were dipped at an angle of 70° into the vessel comprising the MB solution (cell + sample + solution) to make sure that its surface is opposed to the UV-lamp radius and the dipped surface is approximately 3 cm × 2 cm. Following that, the cells were subjected to UV-light at various time intervals (i.e., 30, 60, 90, and 120 min). The UV source was a 15 W Philips G15T8 germicidal lamp generating UVC light with a 254 nm wavelength. The cell and the UV-lamp were at a distance of 7 cm from each other [38].

3. Results and discussion

3.1. Structure analysis

Fig. 1 displays the XRD patterns of the bare and F-doped TiO_2 films. For bare TiO_2 and F-doped TiO_2, the characteristic peaks at 2θ values of 25.52°, 38.16°, 48.21°, 54.18°, 55.14° and 62.72° corresponds to the (101), (004), (200), (105), (211), and (204) planes, respectively. All peaks have the characteristics of anatase-phase TiO_2 and in accordance with the tetragonal phase geometry (space-group I41/amd). These peaks are well matched with the JCPDS card No. 98–009-2363. Worth noting, the increase in the peak's intensity in case of the 7% and 14%F-doped TiO_2 indicate the influence of dopant on the films. This is because, in initial solution, the acid plays a role of catalyst to ameliorate the transparency of the solution but a slight decrease in the intensity of 21% F doped TiO_2 sample can also be observed. Same results were obtained by N. Todorava et al. [39].

TiO_2 has a tetragonal crystal system and for this structure; the expression of the inter reticular distance d_{hkl} is given by the standard formula (Eq. (1)).

$$d_{hkl} = \frac{a}{\sqrt{h^2 + k^2 + \frac{a^2}{c^2}l^2}} \quad (1)$$

Where d_{hkl} is d-spacing of the (*hkl*) line. The lattice constants *a* and *c* are calculated from the two lattice planes.

To calculate the crystalline size and strain, we have adopted the Williamson-Hall plots (H-W). The broadening of peaks indicates grain refinement as well as the high strain related to the powder. Using the relation (Eq. (2)), the instrumental width (βhkl) correlating to every diffraction peak intensity of TiO_2 can be adjusted.

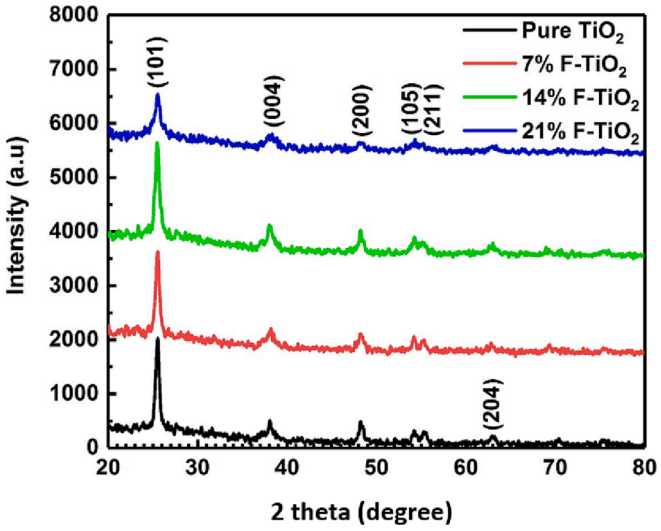

Fig. 1. XRD patterns of undoped and F-doped TiO_2 films.

$$\beta^2_{hkl} = \beta^2_{mesured} - \beta^2_{instrumental} \quad (2)$$

Using the Debye-Scherrer formula (Eq. (3)), we were able to determine the typical size of nanocrystals.

$$D = \frac{k\lambda}{\beta_{hkl}\cos\theta} \quad (3)$$

Where "λ" is the X-ray beam wavelength (Cu-$K_{\alpha 1}$ = 1.5406 Å), β_{hkl} is the full-width at half-maximum (FWHM) of the diffraction peak (*hkl*), $\beta_{instumental}$ is the FWHM attributed to the instrumental-contribution, and θ is the Bragg-angle.

The powders strain caused by the crystal distortion and imperfection was computed via the following formula (Eq. (4)):

$$\varepsilon = \frac{\beta_{hkl}}{4\tan\theta} \quad (4)$$

According to Eqs. (3) and (4), the peak width from particle sizes varies as (1/cosθ) and strain changes as tanθ. Considering that the effects of particle size and strain on line broadening are irrespective of one another and follow a Cauchy-like profile, the obtained line width is just the sum of Eqs. (3) and (4) as revealed in Eq. (5).

$$\beta_{hkl} = \frac{K\lambda}{D\cos\theta} + 4\varepsilon\tan\theta \quad (5)$$

By reordering the equation in the previous sentence, we can get Eq. (6) as follows;

$$\beta_{hkl}\cos\theta = \frac{K\lambda}{D} + 4\varepsilon\sin\theta \quad (6)$$

The equations that have been presented so far are W-H equations. After performing a linear fit to the data, a plot is generated with 4sinθ along the x-axis and β_{hkl} cosθ along the y-axis. The crystallite size was determined from the y-intercept, while the strain ε was determined from slope of the fit. The uniform-deformation-model (UDM) represented by the equation (Eq. (6). In this model, the strain was supposed to be the same in all crystallographic-directions. By doing so, the crystal isotropic nature was taken into consideration. In an isotropic crystal, the properties of the materials are not affected by the direction in which they are assessed. Table 1 provides a concise summary of the outcomes that were collected.

The degree of preferred orientation $T_{(hkl)}$ was utilized for the purpose of conducting research on the texture of films with varying thicknesses. The following mathematical equation (Eq. (7)) can be used to get the value of this factor [40]:

$$T_{(hkl)} = \frac{I_{m(hkl)}/I_{0(hkl)}}{\left(\frac{1}{N}\right)\sum_1^N I_{m(hkl)}/I_{0(hkl)}} \quad (7)$$

Where T(hkl) represents the texture coefficient (TC) of the (*hkl*) plane, I_m(hkl) represents the determined intensity of the (*hkl*) plane, I_0(hkl) represents the analogous documented intensity of the typical TiO_2 using JCPDS Card No. 98–009-2363, and N represents the preferable growth direction. It can be seen from the plots in Fig. 2, that the TC for each peak is inferior or close to unity (T (*hkl*) ≤ 1), except (0 0 4) and (1 0 5) which shows a high TC (>1) in case of 7%F-TiO_2 and 14%F-TiO_2 samples, but TC (0 0 4) > TC (1 0 5), indicating that (0 0 4) reveals a particular preferential orientation for crystallization. In case of 21%F-TiO_2, the (1 0 5)

Table 1
Structural constraints of undoped and F-doped TiO_2 thin films.

	Crystallite parameters		HAL-WILIAMSON PLOTS	
	a = b (Å)	c(Å)	Crystallite size (nm)	Lattice strain %
TiO_2-0F	3.7677	9.4257	15.9	0.1(3)
TiO_2-7%F	3.7727	9.4860	11.5	0.1(3)
TiO_2-14%F	3.7749	9.4787	14.9	0.1(3)
TiO_2-21%F	3.7757	9.4724	10.7	−0.6(2)

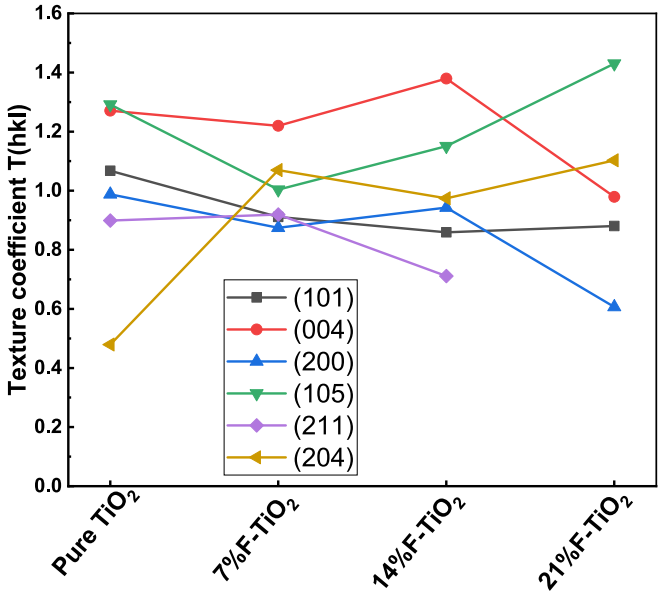

Fig. 2. The calculated texture coefficient of undoped and F-doped TiO_2 films.

shows a high texture coefficient, indicating that the high percentage of Fluorine dopant can influence the preferential orientation crystallization. The pure TiO_2 reveals a preferred crystallization in both (0 0 4) and (1 0 5) directions.

3.2. Surface morphology

The SEM micrographs of the as-fabricated undoped and F-doped TiO_2 thin films are provided in Fig. 3. The images show many thin layers cracked on top of each other. The texture of the TiO_2 films is made up of many mud-crack like layers and dry river-bed like layers. These cracks are essentially linked to the heat treatment of deposited films (rapid drying at 400 °C and annealing at 500 °C for 1 h) and the variation between the coefficient of expansion of the substrate and the materials deposited (thin layer of doped and undoped TiO_2). Also, we observed that these layers are flat and not concave which means good adhesion of the films. For the undoped TiO_2 film (Fig. 3a), the layers in the form of mud cracks are more intense and smaller than the others (Fig. 3b-d), and the intensity of these cracks decreased with the increase in fluorine content. In previous literature by S. Demirci et al. [41] same structure for F-doped TiO_2 thin films was observed.

The chemical surface composition of undoped and F-doped TiO_2 is characterized by energy-dispersive X-ray spectroscopy and the obtained results are provided in the Table 2. In Table 2, we can see the absence of fluorine and the reduction of glass substrate composition such as Si, Na, and Ca. High percentage of oxygen is remarked which can relate to the glass substrate and a significant increase in carbon percentage is remarked.

To further clarify the effect of F doping on the surface chemistry of TiO_2 films, we used AFM to examine their surface properties. The TiO_2 film surface exhibits a high density of nanoscale peaks with spherical shapes that are unevenly dispersed (Fig. 4). The surface of a 7% F:TiO_2 film has nanosized peaks, but they are less spherical and exhibit lower density than pure TiO_2 films. We found virtually no nano peaks in the 7% F-TiO_2 and 14% F-TiO_2 samples.

The films surface morphology was further mathematically quantified using Gwyddion software [42], and the relevant data is provided in Table 3. The Rms roughness value falls dramatically with increase in the F doping level from 1.986 nm (for bare TiO_2) to roughly 436.341 pm for 21% F-TiO_2. This reflects the smoothness of the texture of the latter film (Table 3). Furthermore, both films exhibit positive surface skewness,

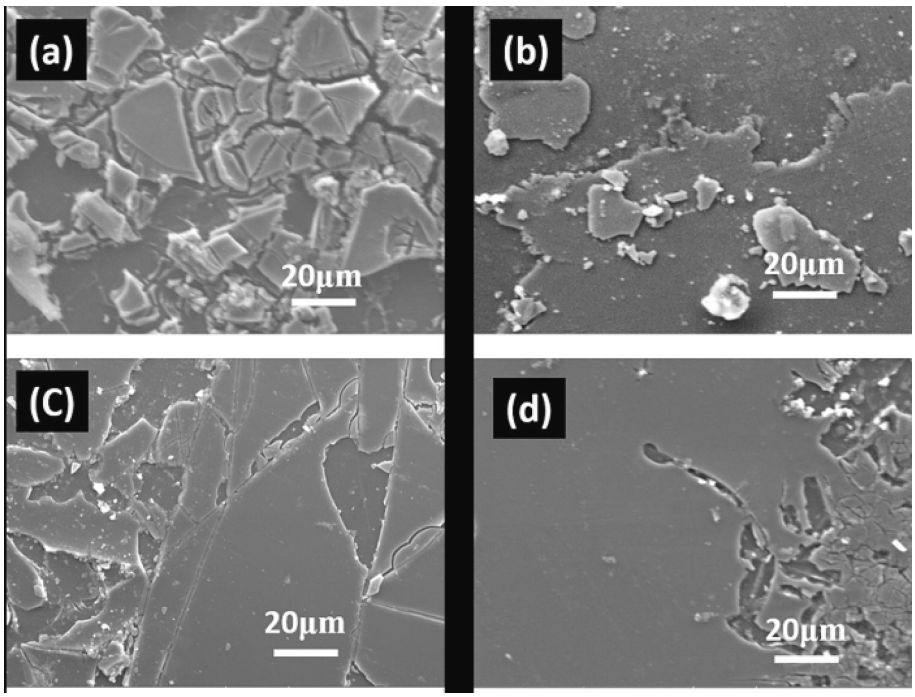

Fig. 3. SEM micrographs of (a) undoped TiO_2 film, (b) 7% F-TiO_2, (c) 14%F-TiO_2 and (d) 21%F-TiO_2 film.

Table 2
Atomic concentration of elements in selected samples.

	Ti (at. %)	O (at. %)	Si (at. %)	Na (at. %)	Ca (at. %)	C (at. %)
Pure TiO_2	4.50	36.34	24.36	7.58	3.42	18.36
7%F-TiO_2	4.50	35.30	24.36	7.58	3.42	18.36
14%F-TiO_2	4.50	33.80	23.06	6.53	3.14	24.00
21%F-TiO_2	7.09	33.30	17.64	4.88	2.40	29.92

confirming the existence of multiple bumps. Such type of nanostructure films, especially the bare TiO_2, would positively influence the permeability thereby having a direct impact on its photodegradation capabilities, in addition to its larger surface area (greater number of nano peaks) and roughness.

3.3. XPS analysis

The X-ray photoelectron spectroscopy (XPS) mainly used for chemical analysis is a commonly employed method and falls within the broad category of surface analysis techniques. The TiO_2 surfaces and interfaces are important in a variety of technical applications, including catalysis regulators, photocatalysis, and gas sensors. Although a precise understanding of the XPS binding energies of various oxidation states is required for XPS analysis of TiO_2. The XPS survey Al K wide-scan spectra of undoped and F-doped TiO_2 films with a pass energy of 200 eV are shown in Fig. 5. The C 1s is related to the adventitious carbon, and the OKLL, Ti LMM, and C KLL auger peaks were produced at binding energy values of 976, 1104, and 1224.12 eV, respectively.

The high resolution XPS spectra of undoped and F-doped TiO_2 films are revealed in Fig. 6. Several Gaussian fits were used to fit the XPS peaks of Ti 2p and O 1s. For backgrounds (BGs), that show only a small increase underneath the peak, a Shirley or Linear BG subtraction is sufficient, therefore Shirley BGs have been used for Ti 2p and O 1s. The pure TiO_2 peaks (Ti 2p and O 1s) have remarkable symmetry, with no shoulders found at lower energies. These symmetrical Ti 2p peaks imply the creation of defect-free stoichiometric TiO_2. The spin orbital splitting produces the doublet Ti $2p_{3/2}$ (460.2 eV) and Ti $2p_{1/2}$ (465.3 eV) in this spectrum. These peaks are comparable with Ti^{4+} in a TiO_2 lattice, and the spin orbital separation between these two peaks is $\Delta T^{4+}2p = 5.05$ eV, almost similar to the previous report [43]. The O 1S of pure TiO_2 is centered at 533.3 eV, which is believed to be induced by bulk oxygen in TiO_2, and same results was reported by S. Karthick et al [44]. Several components of the relative tilt to the higher binding energy side of the peak arose from the TiO_2 surface hydroxylation (when mounted, electrode exposure to air) and the sample preparation procedure.

For F-doped TiO_2 thin films; we can observe that the XPS signal is completely different than the pure TiO_2 and the dopant has a clear effect on the chemical state of elements 'O' and 'Ti', and no binding energy signals of the F 1s can be observed in the range of 688–689 eV. For all doped samples, the peak of O 1s observed at 533.3 eV for pure TiO_2 is deconvoluted into two peaks i.e., 531.1/534.1 eV; 531.6/534.7 eV and 530.9/ 534.0 eV for TiO_2-7%F; TiO_2-14%F and TiO_2-21%F films respectively. The binding energy peak of O 1s at ≈ 531 eV is accredited to the O_2^- in $Ti^{3+}-$ O, and O 1s at ≈ 534 eV is related to the $Ti^{4+}-$ O which is associated with the presence of point defects in TiO_2, such as oxygen vacancies [45], or the presence of adsorbed oxygen. The XPS signal of Ti 2p shows multiple peaks related to T^{4+} and Ti^{3+} oxidation states (see Fig. 6). The Ti^{3+} ($2p_{3/2}$, $2p_{1/2}$) peaks for 7%F-TiO_2, 14%F-TiO_2 and 21%F-TiO_2 are observed at 459.9 and 466.3 eV, 460.56 and 466.9 eV, and 459.7 and 466.1 eV, respectively. The binding energy peaks of Ti^{4+} ($2p_{3/2}$, $2p_{1/2}$) for 7%F-TiO_2, 14%F-TiO_2 and 21%F-TiO_2 are found at 463.1 and 468.4 eV, 463.7 and 469.2 eV, and 463.03 and 468.24 eV, respectively. The XPS spectra depicts that the spin-orbital splitting of the Ti 2p level for F-doped TiO_2 reveals a slight shift to the higher energy side because of the high electronegativity of fluorine than the oxygen. Moreover, any deconvoluted peaks can't be related to the Ti metallic atoms because XRD analysis only shows the presence of the anatase phase of TiO_2 [46]. The distinctive satellite peaks of Ti at 474.8, 475.2, and 474.3 eV for 7%F-TiO_2, 14%F-TiO_2 and 21%F TiO_2 respectively, corresponds to the surface plasmon energy and the binding energy difference between E(satellite) and E($Ti^{4+}p_{3/2}$)≈ 11.5 eV, smaller in comparison to those of the previous reports [47,48], because the displacement of the Ti2p and O1s peaks occurred toward the higher

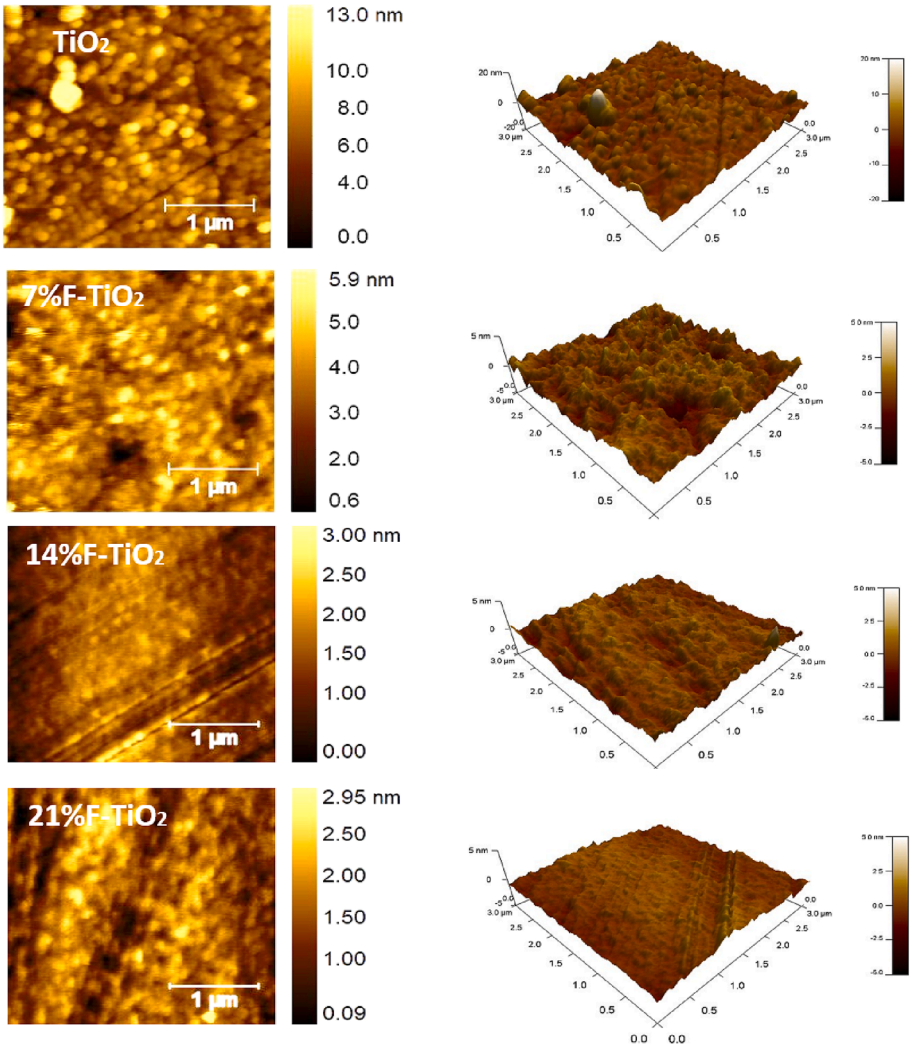

Fig. 4. The 2D and 3D AFM image of: (a) undoped TiO_2, (b) 7% F-doped TiO_2, (c) 14% F-doped TiO_2 and (d) 21% F-doped TiO_2.

Table 3
Roughness constraints for TiO_2 films obtained via AFM image analysis. The roughness constraints include roughness average (Ra), root-mean square surface roughness (RMS), surface skewness (Rsk), and surface kurtosis (Rku).

Compound	Roughness R_{MS}	Skewness R_{sk}	Kurtosis R_{ku}
TiO_2	1.986 nm	1.94	10.6
7%F- TiO_2	651.063 pm	−0.287	0.897
14%F- TiO_2	479.717 pm	0.166	0.655
21%F- TiO_2	436.341 pm	0.052	−0.376

binding energy sides.

3.4. Optical properties

The optical spectra transmittance T(k) in the UV–VIS-NIR spectral area was measured at normal incidence (i.e., 200–1100 nm). As seen in Fig. 7, the spectra reveal a strong interference in the region of 300–1000 nm, with a significant drop in transmittance near the band edge. The interference appearance shows that the deposited coatings are homogeneous. The transmittance shows a highly stable transparency in the visible light region and the average value of transmittance is 85%. In the visible region, when the defects increases, the absorption takes maximum values and the transmittance decreases [49]. In this case, we can conclude that the incorporation of fluorine has not created defects in the structure.

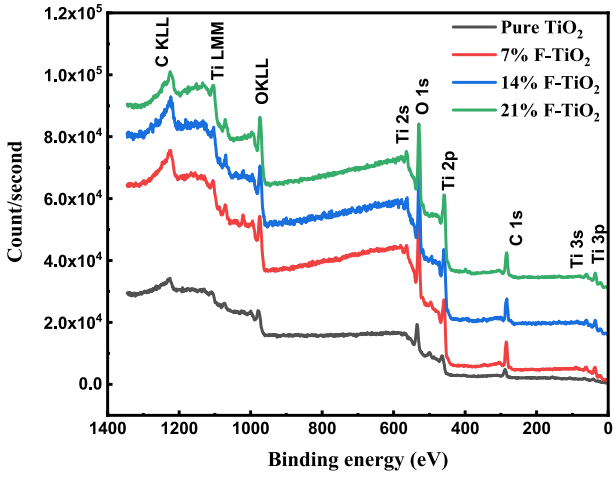

Fig. 5. XPS survey spectra of the undoped and F-doped TiO_2.

The refractive index distribution is significant in optical communication and optical device design. As a result, determining the distribution parameters of the films is critical. Using Eq. (8), the spectral absorbance $A(\lambda)$ is determined from the experimental results [50].

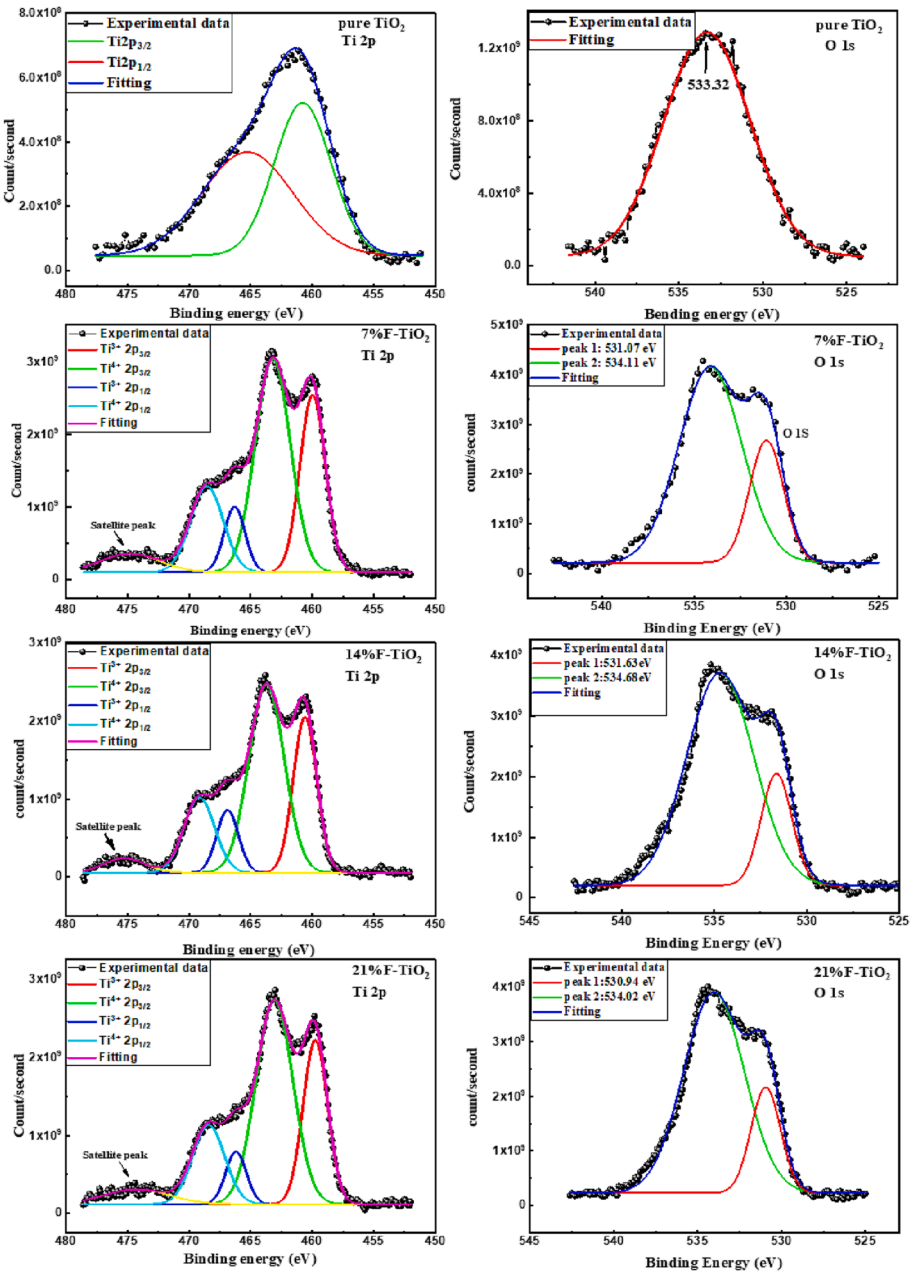

Fig. 6. High resolution XPS of Ti 2p and O 1s core level of undoped TiO_2 and F-doped TiO_2 thin films.

$$A(\lambda) = ln\frac{1}{T(\lambda)} \tag{8}$$

As the absorption coefficient (α) = A/d, the absorbance is proportional to α, where d stands for the films thickness. The indirect band gap (E_g) is determined using the renowned energy exponential relationship (Eq. (9)) [51].

$$AE = A_{Op}(E - E_g)^2 \tag{9}$$

Where A_{Op} is a sample-specific constant. As shown in Fig. 8, the $(AE)^{0.5}$ plot versus E by means of the Tauc approach yield the indirect band gap (E_g) values.

The obtained results reveal that the band gap of pure TiO_2 is 3.24 eV, and it is increased to 3.40, 3.41, and 3.42 eV for the 7, 14, and 21% F-doped samples, respectively. The Moss-Burstein theory correlates the direct or indirect band gaps of a degenerate photocatalyst to the free electrons concentration in its conduction band, predicts that the optical band gap of degenerately doped semiconductors will widen as more of the states close to the conduction band become populated (n_{el}); $Eg \sim n_{el}^{1/3}$.

Using the transmittance-spectrum and the approaches of Manifacier [52] and Swanepoel [53] optical refractive index n(λ) of the undoped and F-doped TiO_2 film were calculated (Fig. 9).

In this case, λ denotes the wavelength. The refractive index is found by drawing two envelopes via the transmittance's maxima $T_M(\lambda)$ and minima $T_m(\lambda)$, respectively as shown by Eqs. (10)–(12).

$$n_\lambda = \sqrt{s + \sqrt{(s^2 - n_s^2(\lambda)}} \tag{10}$$

$$S = \frac{1 - n_s^2(\lambda)}{2} + 2n_S\frac{T_{max}(\lambda) - T_{min}(\lambda)}{T_{max}(\lambda)T_{min}(\lambda)} \tag{11}$$

$$t = \frac{(2K+1)\lambda}{4n_\lambda} \tag{12}$$

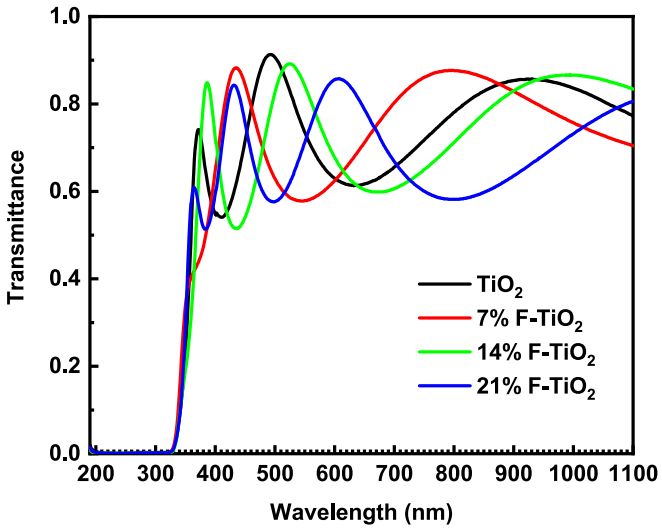

Fig. 7. The spectra of the optical transmittance T(λ).

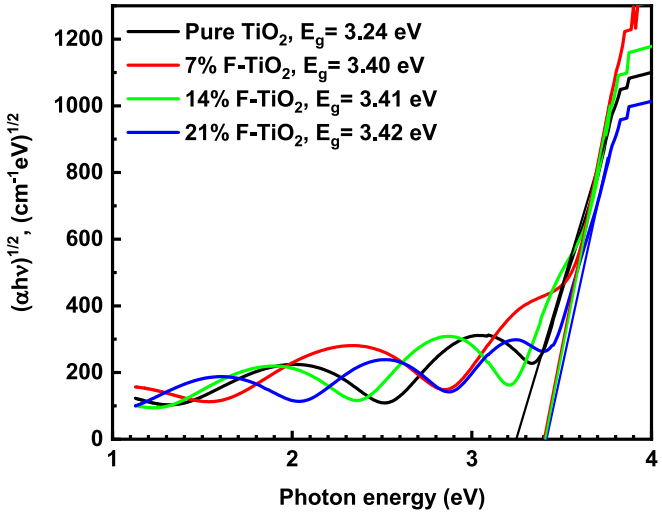

Fig. 8. Optical band gaps of undoped and F-doped TiO_2 thin films.

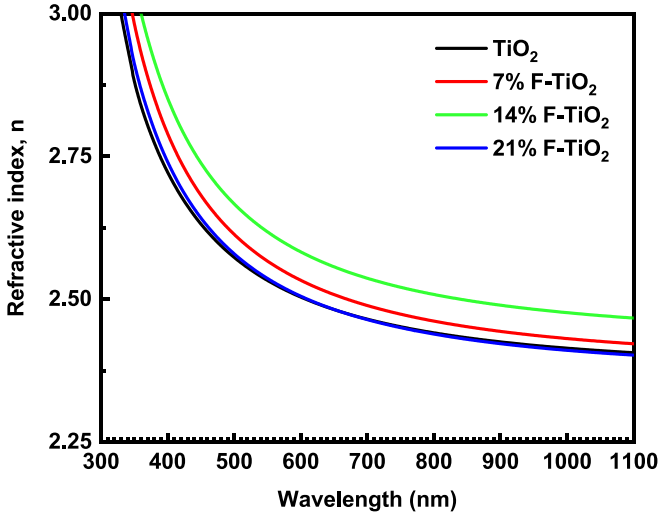

Fig. 9. Refractive index of undoped and F-doped TiO_2 films.

Here, "n_s" represents refractive index of the substrate, where T_{max} and T_{min} represents the largest and smallest possible envelopes, respectively. The film's thicknesses were modified to get optimal fits to the spectral measurements. The values of d, E_g, n at 598 nm, and n_∞ extracted by fitting the experimental data are provided in Table 4. Based on the data collected, it can be concluded that the refractive index is settling into a region very close to that of the anatase phase (2.50–2.58) [54]. Moreover, the band gap (E_g) has not been affected by the fluorine dopant. We found that the optical parameters are not influenced by the fluorine dopant, indicating that the F^- did not create defects or structural change.

3.5. Photocatalytic tests

The photocatalytic activity of the TiO_2 photocatalyst mainly depends on the morphology and structural features. The concentration of fluorine doped TiO_2 factor has been selected to study the MB dye photocatalytic degradation. With fluorine-doped and undoped TiO_2 thin films immersed into methylene blue, the blue color fades at different degrees under ultraviolet irradiation. The optical absorption spectra of MB degradation for all films following the UV light irradiation at various exposure times in the range of 500 to 750 nm are presented in Fig. 10.

Beer- Lambert's law (Eq. (13)) can be used to calculate the percentage of MB degradation from the linear decrease in maximum absorbance with time at 663 nm [38]:

$$rate(\%) = [(C_0 - C_t)/C_0] \times 100 \tag{13}$$

Where C_t and C_0 are the concentrations of the MB solution after and before irradiation at 663 nm.

In Fig. 11, we compare the MB degradation rate of undoped and F-doped TiO_2 thin films as a function of different time exposure. It can be seen that fluorine has a negative effect on the photocatalytic degradation rate. Under UV light exposure, all films show significant MB degradation. The photocatalytic degradation over pure TiO_2, 7% F-TiO_2, 14% F- TiO_2 and 21% F- TiO_2, after 120 min irradiation is 80.97, 82.36, 50.99, and 58.47%, respectively. We can also notice that 7%F-TiO_2 shows a slightly higher degradation rate than the pure TiO_2 but during the first hour (60 min), the pure TiO_2 quickly decomposed the MB dye and revealed a high photocatalytic degradation rate, (i.e., 62% for TiO_2 vs 35.20% for 7%-TiO_2).

The Langmuir-Hinshelwood process is the most suitable for describing heterogeneous photocatalysis, which rely on the electron-hole pairs generation by photo-excitation of the catalyst. Langmuir-Hinshelwood (LH) can be simply expressed by following equations [55,56]. In this model, the rate of reaction (r) is proportional to the fraction of surface covered by the substrate (θ).

$$r = \frac{-dC}{dt} = k\theta \tag{14}$$

Considering Langmuir's equation:

$$\theta = KC/(1 + KC) \tag{15}$$

$$r = \frac{-dC}{dt} = kKC/(1 + KC) \tag{16}$$

Since k is the true rate constant, which takes into account several

Table 4
Dispersion parameters of the bare and F-doped TiO_2 films extracted by fitting the experimental data.

	D Thickness (nm)	E_g (eV)	n at 598 nm	n_∞
TiO_2	192	3.24	2.50	2.37
7%F-TiO_2	160	3.40	2.53	2.38
14%F-TiO_2	199	3.41	2.58	2.42
21%F-TiO_2	242	3.42	2.50	2.36

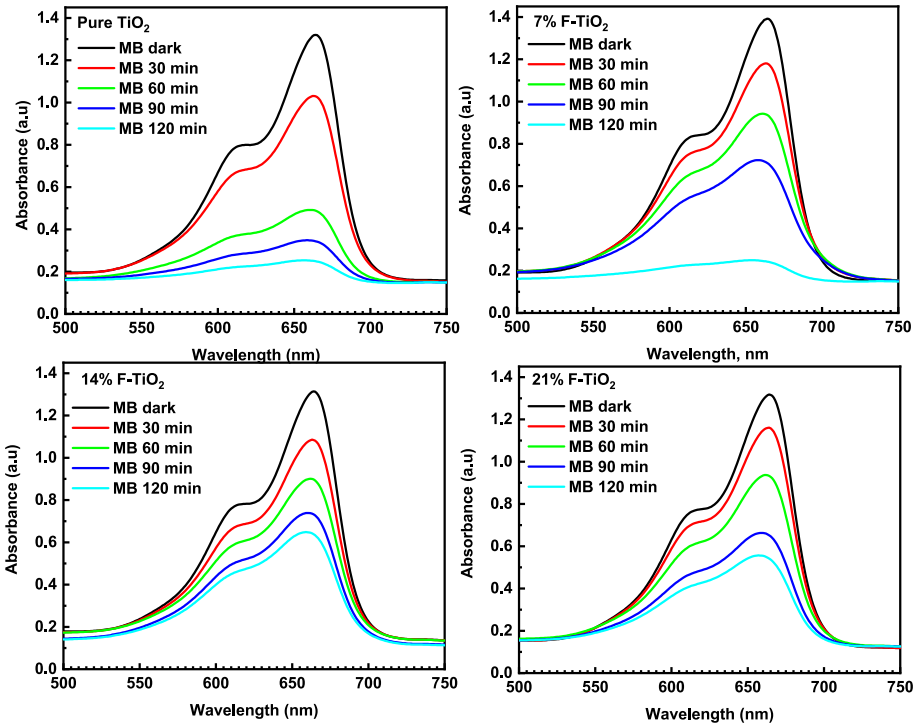

Fig. 10. Absorption spectra of the MB dye concentration measured after photocatalytic reaction over the undoped and F-doped TiO_2 films at different time intervals.

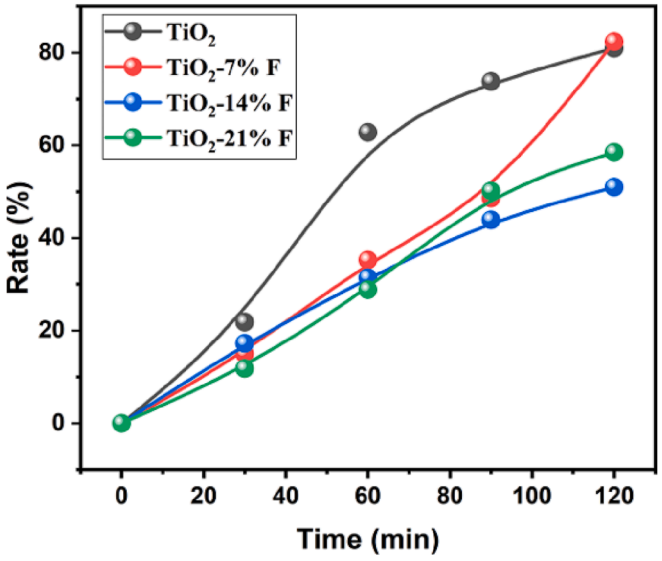

Fig. 11. The MB degradation over the undoped and F-doped TiO_2 thin films as a function of UV-light exposure time.

parameters such as the catalyst's mass, efficient photon flow, O_2 layer, etc., "K" is the constant of adsorption equilibrium of L–H. In photocatalytic studies, the value of "K" is obtained empirically through a kinetic study in the presence of light, and is better than that obtained in the darkness, starting from Langmuir's isotherm. The term "C" is the concentration of the organic substrate at time "t". This equation can be integrated as:

$$Ln\left(\frac{C_0}{C}\right) + K(C_0 - C) = kKt \tag{17}$$

When the solution is highly diluted, C (mol/l) $< 10^{-3}$, the term KC becomes $\ll 1$, the denominator of (Eq. (16)) is neglected and the reaction is essentially an apparent first order reaction.

$$r = \frac{-dC}{dt} = kKC = K_{app}C \tag{18}$$

Where K_{app} stands for the apparent pseudo-first order rate constant. Thus, Eq. (17) can be simplified to a first order reaction when "C_0" is very small, in which case one can be expressed as:

$$Ln\left(\frac{C_0}{C}\right) = K_{app}t \tag{19}$$

The $\ln(C_0/C_t)$ plot vs irradiation time yields the degradation Kinetics reaction. The term "K_{app}" represents slope of the plot for Eq. (19). Fig. 12 depicts the kinetics reaction of MB dye over TiO_2 films with varying sol aging time. The straight-lines are achieved with a linear fitting degree R^2

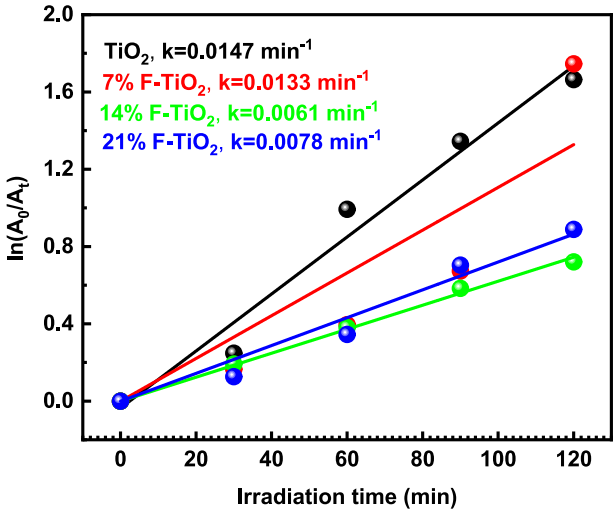

Fig. 12. The reaction rate constant plots of the undoped and F-doped TiO_2 thin films.

of 0.972, 0.897, 0.998 and 0.986 values for TiO_2, 7%F-TiO_2, 14%F-TiO_2 and 21%F-TiO_2, respectively. Further, the spectra reveal that photocatalysis over the undoped and F-doped films is of the first order. The K_{app} (Fig. 12) is also found to decrease with the increase in fluorine content, and same results were obtained by Dozzi et al. [57].

According to our results, we can observe that the rate of degradation decreases when the surface roughness decreases. Several parameters can influence photocatalytic activities, including surface area; surface porosity enhances catalytically active sites, which improves the catalytic performance of semiconductors. Compared to a smoother surface, a rougher surface exhibits better dye degradation. This results was also confirmed by Hsyi-En Cheng et al. [58]. They discovered that, without the effect of heterojunction, TiO_2 coatings on Ni or SnO_2 might have relatively low photocatalytic performance than naked glass due to their lower surface roughness. On the other hand and in the same process, A. Sobczyk-Guzenda et al. [59] showed that Fluorine doped TiO_2 films have a lesser bactericidal effect than pure TiO_2 coatings. In addition, Giannakopoulou et al. [60] found that the amount of fluorine precursor had no effect on the crystallinity or absorption edge of F-doped TiO_2 films.

In addition, another factor that can be taken into consideration is the crystallite size. Let's compare the crystallite size changed by HF addition. We can observe that when the crystallite size decreases from 15.9 nm to 10.7 nm (see Table 1), the MB degradation rate decreases from k = 0.0147 min^{-1} to k = 0.0078 min^{-1} independent of the ratio of HF addition. Wang et al., obtained the same results, where they discovered that increasing the crystallite size of TiO_2 anatase from 6.6 to 26.6 nm, remarkably increase the photocatalytic performance [61], and there is an optimum crystallize size related to several competing effects [62]. These phenomena can be explained by the act of grain boundaries, if the crystallite size decreases, the densities of grain boundaries increase which acts as trapping sites, and decreases the photocatalytic activity. Suzanne et al., demonstrated that the high concentration of strong electron trapping sites at the grain boundaries in TiO_2 impede the transport of electrons between the grains [63] and the presence of fluorine in these grain boundaries in our samples case plays the role of recombination site and decreases the photocatalytic performance and the mobilities of electrons.

4. Conclusion

In this work, high-transparency thin films of TiO_2 have been fabricated via the sol–gel and dip-coating techniques, and the influence of fluoric acid as a source of fluoride ions on the optical, structural, and photocatalytic properties has been explored. We investigated a slight decrease in the crystallinity of 21% F-TiO_2 but didn't observed any affect on the structural parameters of TiO_2. The band gap of fluorine-doped TiO_2 thin films is increased from 3.24 to 3.42 eV, which is related to the change in the chemical states of Ti and O. As a result, same material with different optical properties can be obtained. The surface morphology of TiO_2 remarkably altered and the roughness of the surface considerably decreased with the increase in concentration of HF acid. Thus, the increase in F dopant content remarkably decreased the photocatalytic performance of the TiO_2 photocatalyst related to the decrease in crystallite size.

Funding

This research did not receive any specific grant from funding agencies in the public, commercial, or not-for-profit sectors.

CRediT authorship contribution statement

Abdelaziz Abboudi: Investigation, Visualization, Formal analysis, Writing – original draft. **Sabrina Iaiche:** Methodology, Investigation, Writing – review & editing. **Abdelkader Djelloul:** Visualization, Data curation. **Abdelouahed Chala:** Validation, Formal analysis. **Fouzi Kezzoula:** Validation, Formal analysis. **Fayçal Bensouici:** Conceptualization, Methodology, Supervision, Writing – review & editing. **Mohamed Bououdina:** Conceptualization, Supervision, Writing – review & editing. **Muhammad Humayun:** Conceptualization, Writing – review & editing.

Declaration of Competing Interest

The authors declare that they have no known competing financial interests or personal relationships that could have appeared to influence the work reported in this paper.

Data availability

Data will be made available on request.

Acknowledgements

The authors would like to thank Abbes Laghrour University Khenchela Algeria and Prince Sultan University Riyadh Saudi Arabia for overall support.

References

[1] R.A. Gonçalves, R.P. Toledo, N. Joshi, O.M.J.M. Berengue, Green synthesis and applications of ZnO and TiO_2 nanostructures, Molecules 26 (2021) 2236, https://doi.org/10.3390/molecules26082236.
[2] H.M.S. Al-Aani, E. Iro, P. Chirra, I. Fechete, M. Badea, C. Negrilă, I. Popescu, M. Olea, I.-C. Marcu, Cu_xCeMgAlO mixed oxide catalysts derived from multicationic LDH precursors for methane total oxidation, Appl. Catal. A: Gen. 586 (2019), 117215, https://doi.org/10.1016/j.apcata.2019.117215.
[3] O.M. Ishchenko, G. Lamblin, D. Arl, N. Adjeroud, J. Guillot, P. Grysan, P. Nukala, J. Guyon, I. Fechete, F.J.C.G. Garin, Design, Highly reactive TiO_2 anatase single crystal domains grown by atomic layer deposition, Cryst. Growth Des. 18 (2018) 4929–4936, https://doi.org/10.1021/acs.cgd.8b00170.
[4] M. Humayun, A. Zada, Z. Li, M. Xie, X. Zhang, Y. Qu, F. Raziq, L. Jing, Enhanced visible-light activities of porous $BiFeO_3$ by coupling with nanocrystalline TiO_2 and mechanism, Appl. Catal. B 180 (2016) 219–226, https://doi.org/10.1016/j.apcatb.2015.06.035.
[5] M. Humayun, N. Sun, F. Raziq, X. Zhang, R. Yan, Z. Li, Y. Qu, L. Jing, Synthesis of ZnO/Bi-doped porous $LaFeO_3$ nanocomposites as highly efficient nano-photocatalysts dependent on the enhanced utilization of visible-light-excited electrons, Appl. Catal. B 231 (2018) 23–33, https://doi.org/10.1016/j.apcatb.2018.02.060.
[6] S. Chen, R. Yan, X. Zhang, K. Hu, Z. Li, M. Humayun, Y. Qu, L. Jing, Photogenerated electron modulation to dominantly induce efficient 2,4-dichlorophenol degradation on BiOBr nanoplates with different phosphate modification, Appl. Catal. B 209 (2017) 320–328, https://doi.org/10.1016/j.apcatb.2017.03.003.
[7] M.V. Dozzi, C. D'Andrea, B. Ohtani, G. Valentini, E. Selli, Fluorine-doped TiO_2 materials: photocatalytic activity vs time-resolved photoluminescence, J. Phys. Chem. C 117 (2013) 25586–25595, https://doi.org/10.1021/jp4095563.
[8] M. Humayun, F. Raziq, A. Khan, W. Luo, Modification strategies of TiO_2 for potential applications in photocatalysis: a critical review, Green. Chem. Lett. Rev. 11 (2018) 86–102, https://doi.org/10.1080/17518253.2018.1440324.
[9] M. Humayun, Z. Li, L. Sun, X. Zhang, F. Raziq, A. Zada, Y. Qu, L. Jing, Coupling of nanocrystalline anatase TiO_2 to porous nanosized $LaFeO_3$ for efficient visible-light photocatalytic degradation of pollutants, Nanomaterials 6 (2016) 22, https://doi.org/10.3390/nano6010022.
[10] A. Khlyustova, N. Sirotkin, T. Kusova, A. Kraev, V. Titov, A. Agafonov, Doped TiO_2: the effect of doping elements on photocatalytic activity, Mater. Adv. 1 (2020) 1193–1201, https://doi.org/10.1039/D0MA00171F.
[11] X. Zhang, H. Cui, M. Humayun, Y. Qu, N. Fan, X. Sun, L. Jing, Exceptional performance of photoelectrochemical water oxidation of single-crystal rutile TiO_2 nanorods dependent on the hole trapping of modified chloride, Sci. Rep. 6 (2016) 21430, https://doi.org/10.1038/srep21430.
[12] F. Bensouici, M. Bououdina, A. Dakhel, R. Tala-Ighil, M. Tounane, A. Iratni, T. Souier, S. Liu, W.J.A.S.S. Cai, Optical, structural and photocatalysis properties of Cu-doped TiO_2 thin films, Appl. Surf. Sci. 395 (2017) 110–116, https://doi.org/10.1016/j.apsusc.2016.07.034.
[13] F. Bensouici, T. Souier, A. Dakhel, A. Iratni, R. Tala-Ighil, M. Bououdina, Synthesis, characterization and photocatalytic behavior of Ag doped TiO_2 thin film, Superlattices Microstruct. 85 (2015) 255–265, https://doi.org/10.1016/j.spmi.2015.05.028.
[14] M. Benyakhlef, F. Bensouici, M. Bououdina, A. Dakhel, R. Tala-Ighil, M.J. Toubane, Surface, structural and optical properties dependence of Fe-doped TiO_2 films

deposited onto soda–lime–glass, Surf. Interfaces 21 (2020), 100682, https://doi.org/10.1016/j.surfin.2020.100682.
[15] F. Bensouici, M. Bououdina, A. Dakhel, T. Souier, R. Tala-Ighil, M. Toubane, A. Iratni, S. Liu, W. Cai, Al doping effect on the morphological, structural and photocatalytic properties of TiO_2 thin layers, Thin Solid Films. 616 (2016) 655–661, https://doi.org/10.1016/j.tsf.2016.09.046.
[16] M.K.J. Mohammed, Sol-gel synthesis of Au-doped TiO_2 supported SWCNT nanohybrid with visible-light-driven photocatalytic for high degradation performance toward methylene blue dye, Optik. 223 (2020), 165607, https://doi.org/10.1016/j.ijleo.2020.165607.
[17] K. Selvam, M.J. Swaminathan, Au-doped TiO_2 nanoparticles for selective photocatalytic synthesis of quinaldines from anilines in ethanol, Tetrahedron Lett. 51 (2010) 4911–4914, https://doi.org/10.1016/j.tetlet.2010.07.071.
[18] S.S. Ghumro, B. Lal, T.J. Pirzada, Visible-light-driven carbon-doped TiO_2-based nanocatalysts for enhanced activity toward microbes and removal of dye, ACS Omega 7 (2022) 4333–4341, https://doi.org/10.1021/acsomega.1c06112.
[19] C. Negi, P. Kandwal, J. Rawat, M. Sharma, H. Sharma, G. Dalapati, C.J. Dwivedi, Carbon-doped titanium dioxide nanoparticles for visible light driven photocatalytic activity, Appl. Surf. Sci. 554 (2021), 149553, https://doi.org/10.1016/j.apsusc.2021.149553.
[20] S.A. Ansari, M.M. Khan, M.O. Ansari, M.H. Cho, Nitrogen-doped titanium dioxide (N-doped TiO_2) for visible light photocatalysis, New J. Chem. 40 (2016) 3000–3009, https://doi.org/10.1039/C5NJ03478G.
[21] T.T. Khan, G.A.R. Bari, H.-J. Kang, T.-G. Lee, J.-W. Park, H.J. Hwang, S.M. Hossain, J.S. Mun, N. Suzuki, A.J.C. Fujishima, Synthesis of N-doped TiO_2 for efficient photocatalytic degradation of atmospheric NOx, Catalysts 11 (2021) 109, https://doi.org/10.3390/catal11010109.
[22] Z. Zhang, C. Zhao, Y. Duan, C. Wang, Z. Zhao, H. Wang, Y.J. Gao, Phosphorus-doped TiO_2 for visible light-driven oxidative coupling of benzyl amines and photodegradation of phenol, Appl. Surf. Sci. 527 (2020), 146693, https://doi.org/10.1016/j.apsusc.2020.146693.
[23] D.-D. Qin, Q.-H. Wang, J. Chen, C.-H. He, Y. Li, C.-H. Wang, J.-J. Quan, C.-L. Tao, X.-Q. Lu, Phosphorus-doped TiO_2 nanotube arrays for visible-light-driven photoelectrochemical water oxidation, Sustain, Energy Fuels 1 (2017) 248–253, https://doi.org/10.1039/C6SE00045B.
[24] N. Li, X. Zhang, W. Zhou, Z. Liu, G. Xie, Y. Wang, Y.J. Du, High quality sulfur-doped titanium dioxide nanocatalysts with visible light photocatalytic activity from non-hydrolytic thermolysis synthesis, Inorg. Chem. Front. 1 (2014) 521–525, https://doi.org/10.1039/C4QI00027G.
[25] S.A. Etghani, E. Ansari, S. Mohajerzadeh, Evolution of large area TiS_2-TiO_2 heterostructures and S-doped TiO_2 nano-sheets on titanium foils, Sci. Rep. 9 (2019) 17943, https://doi.org/10.1038/s41598-019-53651-y.
[26] P. Niu, G. Wu, P. Chen, H. Zheng, Q. Cao, H.J. Jiang, Optimization of boron doped TiO_2 as an efficient visible light-driven photocatalyst for organic dye degradation with high reusability, Front. Chem. 8 (2020) 172, https://doi.org/10.3389/fchem.2020.00172.
[27] C. Ni, Y. Tang, H.R. Abdellatif, X. Huang, D. Xie, J. Ni, Boron-doped TiO_2 from anodization of TiB_2 for efficient photocatalysis, J. Electrochem. Soc. 167 (2020), 126505, https://doi.org/10.1149/1945-7111/abad67.
[28] E.M. Samsudin, S.B. Abd Hamid, J.C. Juan, W.J. Basirun, G.J. Centi, Synergetic effects in novel hydrogenated F-doped TiO_2 photocatalysts, Appl. Surf. Sci. 370 (2016) 380–393, https://doi.org/10.1016/j.apsusc.2016.02.172.
[29] J. Xu, Y. Ao, D. Fu, C.J. Yuan, Low-temperature preparation of F-doped TiO_2 film and its photocatalytic activity under solar light, Appl. Surf. Sci. 254 (2008) 3033–3038, https://doi.org/10.1016/j.apsusc.2007.10.065.
[30] T. Morikawa, R. Asahi, T. Ohwaki, K. Aoki, Y.J. Taga, Band-gap narrowing of titanium dioxide by nitrogen doping, Jap. J. Appl. Phys. 40 (2001) L561, https://doi.org/10.1143/JJAP.40.L561.
[31] H. Irie, Y. Watanabe, K.J.T.J.o.P.C.B. Hashimoto, Nitrogen-concentration dependence on photocatalytic activity of $TiO_{2-x}N_x$ powders, J. Phys. Chem. B 107 (2003) 5483-5486. https://doi.org/10.1021/jp030133h.
[32] T. Ihara, M. Miyoshi, Y. Iriyama, O. Matsumoto, S. Sugihara, Visible-light-active titanium oxide photocatalyst realized by an oxygen-deficient structure and by nitrogen doping, Appl. Catal. B 42 (2003) 403–409, https://doi.org/10.1016/S0926-3373(02)00269-2.
[33] C. Minero, G. Mariella, V. Maurino, E. Pelizzetti, Photocatalytic transformation of organic compounds in the presence of inorganic anions. 1. Hydroxyl-mediated and direct electron-transfer reactions of phenol on a titanium dioxide− fluoride system, Langmuir 16 (2000) 2632–2641, https://doi.org/10.1021/la9903301.
[34] W. Yu, X. Liu, L. Pan, J. Li, J. Liu, J. Zhang, P. Li, C. Chen, Z. Sun, Enhanced visible light photocatalytic degradation of methylene blue by F-doped TiO_2, Appl. Surf. Sci. 319 (2014) 107–112, https://doi.org/10.1016/j.apsusc.2014.07.038.
[35] P.-P. Filippatos, A. Soultati, N. Kelaidis, C. Petaroudis, A.-A. Alivisatou, C. Drivas, S. Kennou, E. Agapaki, G. Charalampidis, A.R.b.M. Yusoff, Preparation of hydrogen, fluorine and chlorine doped and co-doped titanium dioxide photocatalysts: A theoretical and experimental approach, J Sci. Rep. 11 (2021) 5700. https://doi.org/10.1038/s41598-021-81979-x.
[36] N. Fessi, M.F. Nsib, L. Cardenas, C. Guillard, F.d.r. Dappozze, A. Houas, F. Parrino, L. Palmisano, G. Ledoux, D.J. Amans, Surface and electronic features of fluorinated TiO_2 and their influence on the photocatalytic degradation of 1-methylnaphthalene, J. Phys. Chem. C 124 (2020) 11456-11468. https://doi.org/10.1021/acs.jpcc.0c01929.
[37] A.M. Díez, I. Núñez, M. Pazos, M.Á. Sanromán, Y.V.J.C. Kolen'ko, Fluoride-doped TiO_2 photocatalyst with enhanced activity for stable pollutant degradation, 12 (2022) 1190. https://doi.org/10.3390/catal12101190.
[38] F. Bensouici, T. Souier, A. Iratni, A. Dakhel, R. Tala-Ighil, M. Bououdina, Effect of acid nature in the starting solution on surface and photocatalytic properties of TiO_2 thin films, Surf. Coat. Technol. 251 (2014) 170–176, https://doi.org/10.1016/j.surfcoat.2014.04.021.
[39] N. Todorova, T. Giannakopoulou, T. Vaimakis, C. Trapalis, Structure tailoring of fluorine-doped TiO_2 nanostructured powders, Mater. Sci. Eng. B 152 (2008) 50–54, https://doi.org/10.1016/j.mseb.2008.06.019.
[40] S. Lemlikchi, S. Abdelli-Messaci, S. Lafane, T. Kerdja, A. Guittoum, M.J. Saad, Study of structural and optical properties of ZnO films grown by pulsed laser deposition, Appl. Surf. Sci. 256 (2010) 5650–5655, https://doi.org/10.1016/j.apsusc.2010.03.026.
[41] S. Demirci, T. Dikici, M. Yurddaskal, S. Gultekin, M. Toparli, E.J. Celik, Synthesis and characterization of Ag doped TiO_2 heterojunction films and their photocatalytic performances, Appl. Surf. Sci. 390 (2016) 591–601, https://doi.org/10.1016/j.apsusc.2016.08.145.
[42] D. Nečas, P.J. Klapetek, Gwyddion: an open-source software for SPM data analysis, Open Phys. 10 (2012) 181–188, https://doi.org/10.2478/s11534-011-0096-2.
[43] R. Nawaz, C.F. Kait, H.Y. Chia, M.H. Isa, L.W.J.N. Huei, Glycerol-mediated facile synthesis of colored titania nanoparticles for visible light photodegradation of phenolic compounds, Nanomaterials 9 (2019) 1586, https://doi.org/10.3390/nano9111586.
[44] S. Karthick, K. Prabakar, A. Subramania, J.-T. Hong, J.-J. Jang, H.-J.J.P.t. Kim, Formation of anatase TiO_2 nanoparticles by simple polymer gel technique and their properties, Powder Technol. 205 (2011) 36-41. https://doi.org/10.1016/j.powtec.2010.08.061.
[45] P. Gu, X. Zhu, H. Wu, J. Li, D. Yang, Influence of oxygen vacancy on the response properties of TiO2 ultraviolet detectors, J. Alloys. Compd. 779 (2019) 821–830, https://doi.org/10.1016/j.jallcom.2018.11.283.
[46] M. Pérez-González, S. Tomás, J. Santoyo-Salazar, M. Morales-Luna, Enhanced photocatalytic activity of TiO_2-ZnO thin films deposited by dc reactive magnetron sputtering, Ceram. Int. 43 (2017) 8831–8838, https://doi.org/10.1016/j.ceramint.2017.04.016.
[47] M. Pérez-González, S. Tomás, Surface chemistry of TiO_2-ZnO thin films doped with Ag. Its role on the photocatalytic degradation of methylene blue, Catal. Today. 360 (2021) 129–137, https://doi.org/10.1016/j.cattod.2019.08.009.
[48] M. Oku, H. Matsuta, K. Wagatsuma, Y. Waseda, S. Kohiki, Removal of inelastic scattering part from Ti2p XPS spectrum of TiO_2 by deconvolution method using O1s as response function, J. Electron Spectrosc. 105 (1999) 211–218, https://doi.org/10.1016/S0368-2048(99)00067-5.
[49] E. Asikuzun, O. Ozturk, L. Arda, C. Terzioglu, Preparation, growth and characterization of nonvacuum Cu-doped ZnO thin films, J. Mol. Struct. 1165 (2018) 1–7, https://doi.org/10.1016/j.molstruc.2018.03.053.
[50] W.Q. Hong, Extraction of extinction coefficient of weak absorbing thin films from special absorption, J. Phys. D 22 (1989) 1384, https://doi.org/10.1088/0022-3727/22/9/024.
[51] F. Abeles, Optical properties of solids, North-Holland Pub, Co, 1972.
[52] J. Manifacier, J. Gasiot, J.J. Fillard, A simple method for the determination of the optical constants n, k and the thickness of a weakly absorbing thin film, J. Phys. E 9 (1976) 1002, https://doi.org/10.1088/0022-3735/9/11/032.
[53] R.J. Swanepoel, Determination of the thickness and optical constants of amorphous silicon, J. Phys. E: Sci. Instrum. 16 (1983) 1214, https://doi.org/10.1088/0022-3735/16/12/023.
[54] W.D. Kingery, H.K. Bowen, D.R. Uhlmann, Introduction to ceramics, John wiley & sons, 1976.
[55] M. Toubane, R. Tala-Ighil, F. Bensouici, M. Bououdina, W. Cai, S. Liu, M. Souier, A. J. Iratni, Structural, optical and photocatalytic properties of ZnO nanorods: effect of aging time and number of layers, Ceram. Int. 42 (2016) 9673–9685, https://doi.org/10.1016/j.ceramint.2016.03.056.
[56] J.P.S. Valente, P.M. Padilha, A.O.J.C. Florentino, Studies on the adsorption and kinetics of photodegradation of a model compound for heterogeneous photocatalysis onto TiO_2, Chemosphere 64 (2006) 1128–1133, https://doi.org/10.1016/j.chemosphere.2005.11.050.
[57] M.V. Dozzi, B. Ohtani, E.J. Selli, Absorption and action spectra analysis of ammonium fluoride-doped titania photocatalysts, Phys. Chem. Chem. Phys. 13 (2011) 18217–18227, https://doi.org/10.1039/C1CP21558B.
[58] H.-E. Cheng, C.-H. Hung, I.-S. Yu, Z.-P.-J. Yang, Strongly enhancing photocatalytic activity of TiO_2 thin films by multi-heterojunction technique, Catalysts 8 (2018) 440, https://doi.org/10.3390/catal8100440.
[59] A. Sobczyk-Guzenda, S. Owczarek, A. Wojciechowska, D. Batory, M. Fijalkowski, M.J. Gazicki-Lipman, Fluorine doped titanium dioxide films manufactured with the help of plasma enhanced chemical vapor deposition technique, Thin Solid Films. 650 (2018) 78–87, https://doi.org/10.1016/j.tsf.2018.01.060.
[60] T. Giannakopoulou, N. Todorova, T. Vaimakis, S. Ladas, C.J. Trapalis, Study of fluorine-doped TiO_2 sol-gel thin coatings, J. Sol. Energy Eng. 130 (2008), https://doi.org/10.1115/1.2969804.
[61] X. Wang, L. Sø, R. Su, S. Wendt, P. Hald, A. Mamakhel, C. Yang, Y. Huang, B. B. Iversen, F. Besenbacher, The influence of crystallite size and crystallinity of anatase nanoparticles on the photo-degradation of phenol, J. Catal. 310 (2014) 100–108, https://doi.org/10.1016/j.jcat.2013.04.022.
[62] I.J. Badovinac, R. Peter, A. Omerzu, K. Salamon, I. Šarić, A. Samaržija, M. Perčić, I. K. Piltaver, G. Ambrožić, M. Petravić, Grain size effect on photocatalytic activity of TiO_2 thin films grown by atomic layer deposition, Thin Solid Films. 709 (2020), 138215, https://doi.org/10.1016/j.tsf.2020.138215.
[63] S.K. Wallace, K.P. McKenna, Grain boundary controlled electron mobility in polycrystalline titanium dioxide, Adv. Mater. Interfaces 1 (2014) 1400078, https://doi.org/10.1002/admi.201400078.